Synthesis of a first-order passive complex filter with band-pass/band-elimination characteristics

Tomoya Nakagawa · Kazuhiro Shouno · Kenji Kuniya

Abstract In this paper, a new passive complex filter is proposed. In the same fashion as the traditional real band-pass filter, the proposed circuit is also designed through the frequency transformation. In order to obtain the prototype complex filter suitable for passive realization, the extended lowpass–highpass transformation or the bilinear lowpass–lowpass transformation different from the well-known frequency shifting method is adopted. These transformations give two filters; however, the final circuits become identical to each other. The proposed circuit has two output terminals. One is the complex band-pass output, and the other is for the complex band-elimination. The proposed circuit includes a capacitor, an autotransformer or an inductor and termination resistors only. Because the proposed circuit has terminating resistors at both of the input and the output sides, it is suitable for high frequency application. As an example, two first-order complex filters which operate in 100 kHz and 10 MHz are designed and their frequency responses are measured. It is shown that the measured frequency responses agree with the theoretical ones through experiment.

T. Nakagawa · K. Shouno (✉) · K. Kuniya
University of Tsukuba, 1-1-1 Tennodai, Tsukuba-shi 305-8573, Japan
e-mail: shouno@cs.tsukuba.ac.jp

T. Nakagawa
e-mail: nakatomo@fillab.is.tsukuba.ac.jp

K. Kuniya
e-mail: kunitika192636@fillab.is.tsukuba.ac.jp

1 Introduction

Recently, many techniques concerned with the complex filters have been proposed [1–12]. Complex filters have frequency responses asymmetrical with respect to the dc axis. This property is important for application in the field of communication systems, such as orthogonal modulation/demodulation, image rejection filters, and so on.

Complex filters are classified into two categories. One is the active realization and the other is the passive realization. The former requires active components such as operational amplifiers, transconductors and so on. The latter can be realized without the active components which limit their operating frequency. Therefore, the passive complex filter has a desirable frequency response over a wide frequency range.

The RC polyphase filters [3–7] can be classified into the passive complex filter. It is attractive from the viewpoint of its integration. However, they require voltage sources with low internal resistance and output buffers with high input impedance. Such amplifiers do not have desirable characteristics especially in the high frequency area. Moreover, this filter inevitably includes resistors in the signal paths. This means that it has some insertion loss.

The signal paths of the passive complex filter using transformers [8–10] include the reactance elements only. In addition, this filter has the termination resistors. Because it requires transformers equipped with two separated windings, its operating frequency becomes relatively low. This problem can be solved by excluding such transformers.

In this paper, a new complex filter is proposed. The proposed filter includes an inductor or an autotransformer and a capacitor only. It is synthesized through extended lowpass–highpass transformation (ELHT) [11] and bilinear lowpass–lowpass transformation (BLLT) [12] specialized for the passive realization. In order to confirm the validity

of the proposed method, two first-order complex filters are designed and their frequency responses are measured. It is shown that these circuits have band-pass and band-elimination characteristics simultaneously through experiment.

2 Proposed method

2.1 Frequency transformation I

Figure 1a shows a first-order real prototype low-pass filter. It should be noted that this circuit does not have a termination resistor at the output side. According to ELHT [11], which is one of the frequency transformation methods that transforms a prototype real low-pass filter into a corresponding complex filter, its frequency transformation is given by

$$x = -\frac{\omega_C}{\omega - \omega_S} - x_S, \tag{1}$$

where x and ω are frequencies of the prototype filter and the destination complex filter, respectively, and ω_C, ω_S and x_s are constants given by design specifications. In order to obtain the prototype filter suitable for passive realization, substituting $\omega_S = 0$ into the above equation yields

$$x = -\frac{\omega_C}{\omega} - x_S. \tag{2}$$

Equation (2) is a special case of the ELHT. Figure 2 shows its transformation. In this figure, $T(jx)$ and $T_C(j\omega)$ are

the transfer functions of the prototype real low-pass filter and the transformed complex filter, respectively. j is an
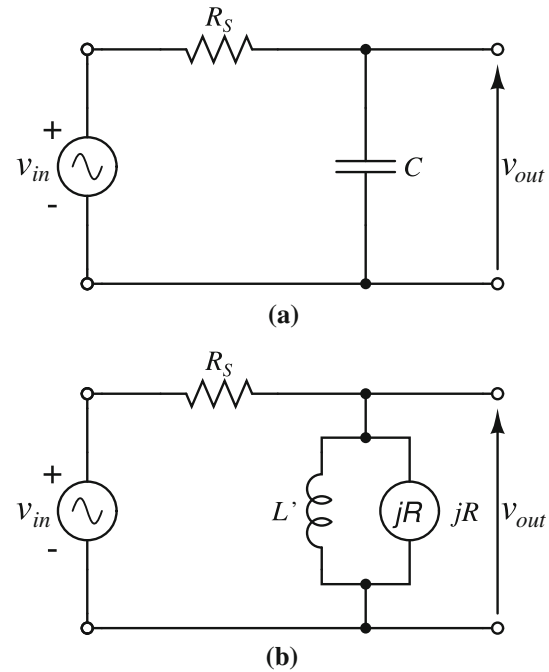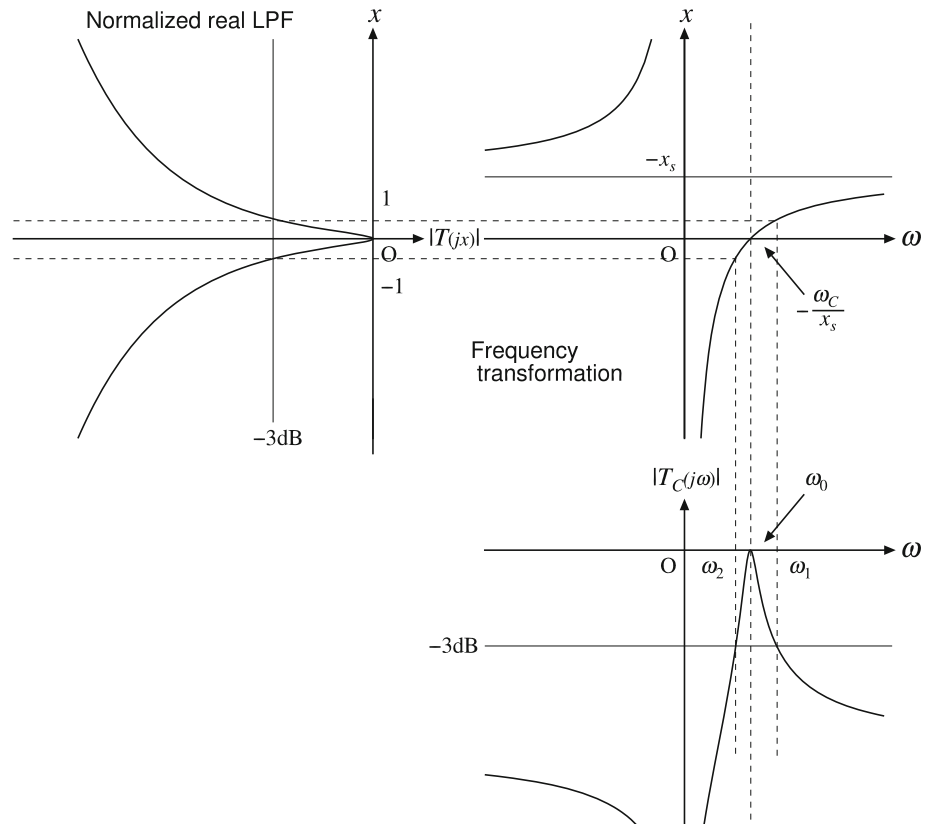

Fig. 1 Synthesis of the complex prototype band-pass filter. a Real prototype low-pass filter. b Complex prototype band-pass filter

Fig. 2 Frequency transformation for complex band-pass filter

imaginary unit. The transfer function $T_C(j\omega)$ has a complex bandpass response. The values of ω_C and x_s are given by

$$\left.\begin{array}{l} \omega_C = \dfrac{\omega_1\omega_0}{\omega_1-\omega_0} = \dfrac{\omega_0\omega_2}{\omega_0-\omega_2} \\ x_S = \dfrac{\omega_1}{\omega_0-\omega_1} = \dfrac{\omega_2}{\omega_2-\omega_0} \end{array}\right\}, \tag{3}$$

where ω_1 and ω_2 are the passband edge frequencies of the destination complex filter, and ω_0 is defined as the following harmonic mean of them, i.e.

$$\frac{2}{\omega_0} = \frac{1}{\omega_1} + \frac{1}{\omega_2}. \tag{4}$$

The value of ω_0 gives the center frequency of the complex bandpass filter. Applying this transformation to the prototype filter shown in Fig. 1(a), we can obtain a complex filter shown in Fig. 1(b).

Through the transformation defined by (2), the capacitor C of the prototype filter is transformed into a parallel circuit of an inductor L' and an imaginary resistor jR. Their element values are

$$\left.\begin{array}{l} L' = \dfrac{1}{\omega_C C} \\ jR = \dfrac{j}{x_S C} \end{array}\right\}. \tag{5}$$

2.2 Realization of imaginary resistor

Figure 3(a) shows an imaginary resistor. The relationship between v and i is given by

$$v = jRi. \tag{6}$$

Decomposing voltage v and current i into their real and imaginary components gives

$$\left.\begin{array}{l} v = v_r + jv_i \\ i = i_r + ji_i \end{array}\right\}, \tag{7}$$

where subscripts r and i denote real and imaginary signal paths, respectively. Substituting the above equation into (6), we have

$$v_r + jv_i = -Ri_i + jRi_r. \tag{8}$$

From the above equation, we have

$$\left.\begin{array}{l} v_r = -Ri_i \\ v_i = Ri_r \end{array}\right\}. \tag{9}$$

We introduce the following v_i' and i_i' given by

$$\left.\begin{array}{l} v_i' = R_0 i_i \\ i_i' = \dfrac{1}{R_0} v_i \end{array}\right\}, \tag{10}$$

where R_0 is an positive constant. From the above equation, we have

$$\left.\begin{array}{l} i_i = \dfrac{1}{R_0} v_i' \\ v_i = R_0 i_i' \end{array}\right\}. \tag{11}$$

(a)

real circuit

(b)

imaginary circuit
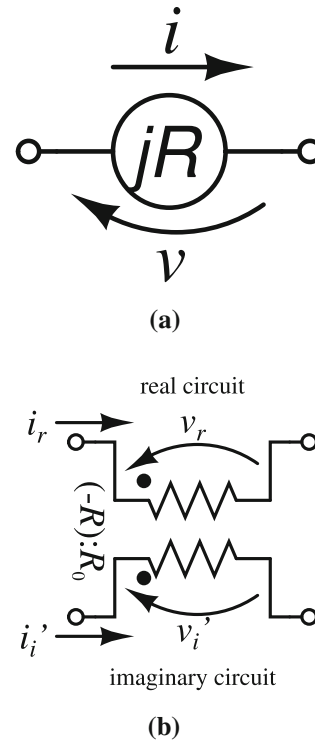
Fig. 3 Realization of imaginary resistor. a Imaginary resistor. b Imaginary resistor realized by using ideal transformer

Substituting this into (9) yields

$$\begin{pmatrix} v_r \\ i_r \end{pmatrix} = \begin{pmatrix} -R/R_0 & 0 \\ 0 & -R_0/R \end{pmatrix} \begin{pmatrix} v_i' \\ -i_i' \end{pmatrix}. \tag{12}$$

This expresses a two-port circuit written in an F matrix form. This indicates an ideal transformer whose turn ratio is $(-R):R_0$ [5]. Figure 3(b) shows the ideal transformer which simulates the imaginary resistor shown in Fig. 3(a).

Equation (11) indicates that the relationship between voltage and current are interchanged in the imaginary circuit. Therefore, the imaginary circuit becomes a dual circuit of the real circuit.

Consequently, the circuit shown in Fig. 1(b) can be equivalently realized by the circuit shown in Fig. 4. In this circuit, v_{ir} and v_{or} are the input and the output signal of the real circuit, respectively, and v_{ii} and i_{oi} represent those of the imaginary circuit. Since the imaginary circuit is dual of the real one, the input signal source of the imaginary circuit becomes the current source v_{ii}/R_0.

2.3 Circuit realization with an autotransformer or an inductor

Because both windings of the ideal transformer surrounded by broken lines in Fig. 4 are grounded and L' is connected to the winding in parallel, they can be realized by a tight coupling transformer whose self inductances are L' and
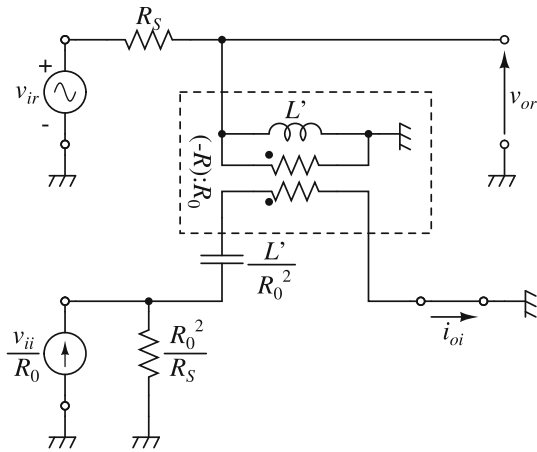
Fig. 4 Complex band-pass filter with an ideal transformer

Fig. 5 Doubly terminated band-pass complex filter with tight coupling transformer

$(R_0/R)^2 L'$. Its equivalent circuits are summarized in Table 1. The proposed circuits can be classified into Type I-A, I-B, I-C and Type II. From this table, it is found that a transformer can be replaced with an autotransformer in many cases.

When $R_0 = -R$ (Type I-C), the autotransformer becomes an inductor. In this case, we have the following condition from (5).

$$x_S = -\frac{1}{R_0 C}. \tag{13}$$

The above equation indicates that the freedom of design flexibility is decreased.

2.4 Addition of termination resistors

The current source v_{ii}/R_0 with internal resistor R_0^2/R_S in Fig. 4 can be equivalently converted into a voltage source $v_{ii} R_0/R_s$ with internal resistor R_0^2/R_S. Moreover, we can add
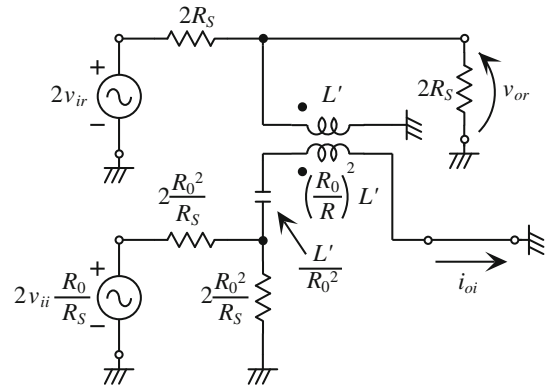
termination resistors to the output side of the circuit shown in Fig. 4 without affecting its frequency response as shown in Fig. 5. According to Thévenin's theorem, it is obvious that the circuits shown in Figs. 4 and 5 are equivalent to each other.

From Table 1, the proposed circuits can be obtained. Figures 6 and 7 show the examples of the proposed circuits using Type I-A and I-C, respectively. In these figures, L_1, L_2 and C'' becomes

$$\left. \begin{array}{l} L_1 = L' \\ L_2 = \left\{ (R_0/R)^2 - 1 \right\} L' \\ C'' = L'/R_0^2 \end{array} \right\}. \tag{14}$$

Because the imaginary output signal i_{oi} of the circuit shown in Fig. 4 is mixed together with another signal, it should be noted that the voltage v_{x1} and v_{x2} shown in Figs. 6 and 7 are not the imaginary output signal. In other words, v_{x1} and v_{x2} are useless signals in this stage. However, as described in the following section, it is

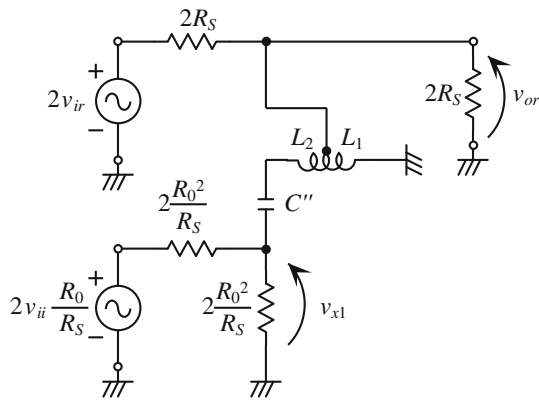**Table 1** Equivalent circuit of tight-coupling transformer

Fig. 6 Proposed complex band-pass filter realized by using an autotransformer (Type I-A)
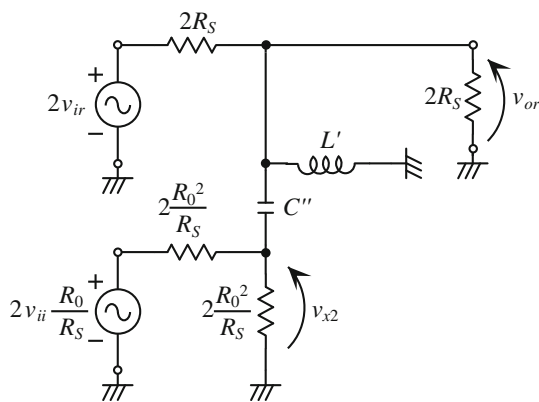

Fig. 7 Proposed complex band-pass filter realized by using an inductor (Type I-C)

shown that the band-elimination response can be obtained from this terminal.

2.5 Frequency transformation II

When BLLT [11] is used, the frequency transformation becomes

$$x = -\frac{1}{-\dfrac{\omega_C}{\omega} - x_S}. \tag{15}$$

In this equation, ω_C and x_s can be decided from (3). Figure 8(a) shows the complex filter obtained through the above transformation. Its element values are given by

$$\left.\begin{array}{l} C' = \dfrac{C}{\omega_C} \\[2mm] jR = -\dfrac{jx_S}{C} \end{array}\right\}. \tag{16}$$

Applying the transformation described in Sects. 2.2, 2.3 and 2.4, we obtain the complex filter shown in Fig. 8(b).

Since the circuits shown in Figs. 4 and 8(b) have the same structure, the proposed circuits have the complex
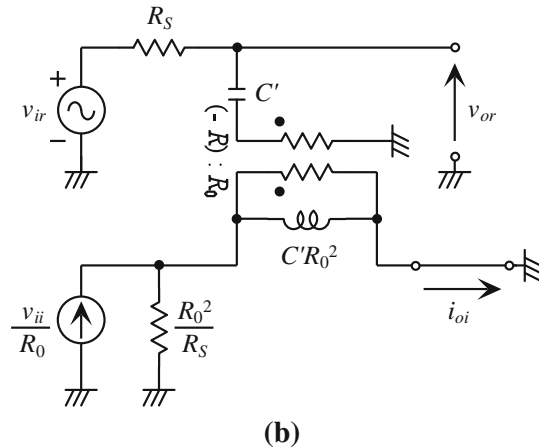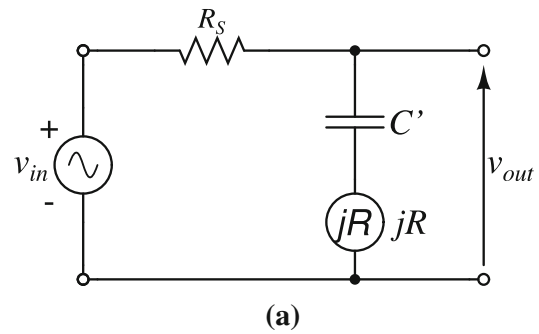

(a)

(b)

Fig. 8 Proposed complex band-elimination filter. **a** Prototype. **b** Complex band-elimination filter with an ideal transformer

band-pass and band-elimination characteristics, simultaneously. For example, if we use the circuit shown in Fig. 6 as a complex band-pass filter, v_{x1} becomes a band-elimination output signal. When the following condition is satisfied, both of the proposed band-pass and band-elimination filters have the same passband edges because the entire element values of the circuits shown in Figs. 4 and 8(b) are identical to each other.

$$C = R_0 = 1. \tag{17}$$

3 Design examples

3.1 Proposed circuit using autotransformer (100 kHz)

We designed a complex filter based on the ELHT described in Sect. 2.1. First, we set the element values of the normalized real low-pass filter shown in Fig. 1(a) to

$$\left.\begin{array}{l} R_S = 1 \\ C = 1 \end{array}\right\}. \tag{18}$$

In the following sections, this element values are adopted. The passband edge frequencies are 1 and -1. At these frequencies, its voltage gain becomes -3 dB. Through the frequency transformation, these frequencies
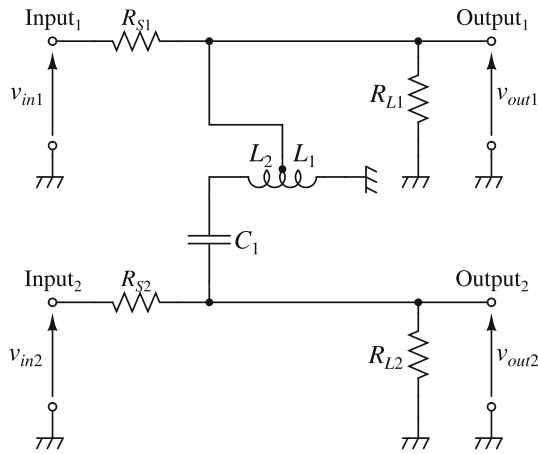
Fig. 9 Experimental circuit using an autotransformer for Type I-A

Table 2 Element values for experiment 1 (Type I-A, 90–110 kHz)

Element	Theoretical	Measured	Turns	Q
R_{S1}	600 Ω	600.0 Ω	–	–
R_{L1}	600 Ω	600.0 Ω	–	–
R_{S2}	600 Ω	600.0 Ω	–	–
R_{L2}	600 Ω	600.0 Ω	–	–
C_1	535.9 pF	0.536 nF	–	>1,000
L_1	48.23 μH	48.06 μH	9	92
L_2	3.907 mH	3.923 mH	81	290

are mapped onto ω_1 and ω_2 which are the passband edge frequencies of the destination complex band-pass filter. We design a complex filter whose passband edges are

$$\left.\begin{array}{l} \omega_1 = 11 \,\text{rad/s} \\ \omega_2 = 9 \,\text{rad/s} \end{array}\right\}. \tag{19}$$

Substituting the above equation set into (3) and (4) yields

$$\left.\begin{array}{l} \omega_0 = 9.9 \\ \omega_C = 99 \\ x_S = -10 \end{array}\right\}. \tag{20}$$

Substituting (18) and (20) into (5) gives

$$\left.\begin{array}{l} L' = 0.0101010 \\ jR = -0.1j \end{array}\right\}. \tag{21}$$

The value of R_0 concerned with the turn ratio of the ideal transformer is usually set to unity for the sake of simplicity. Because the condition (17) is satisfied, the band-elimination characteristics also satisfy the specifications given by (19).

From Table 1, it is found that the autotransformer shown in Type I-A can be used. Figure 9 shows the resultant filter. From (14), element values becomes $L_1 = 0.0101010$, $L_2 = 0.818182$, $C_1 = 0.0101010$ and $R_{S1} = R_{S2} = R_{L1} = R_{L2} = 2$.

Secondly, these element values are scaled such that the operating frequency and the impedance level become 100 kHz and 600 Ω, respectively. The resulting cutoff frequencies are on 90 and 110 kHz. The element values of the experimental circuit are summarized in Table 2. The deviations between the desired and the measured element values are within ±0.7 %. The transformer is realized by using a ferrite pot core H5AP26/16T-32H (TDK), and 0.25 mm φUEW is used for its winding. A polystyrene film capacitor is used. The experimental circuit is implemented on a paper phenolic PCB (t = 1.6 mm).
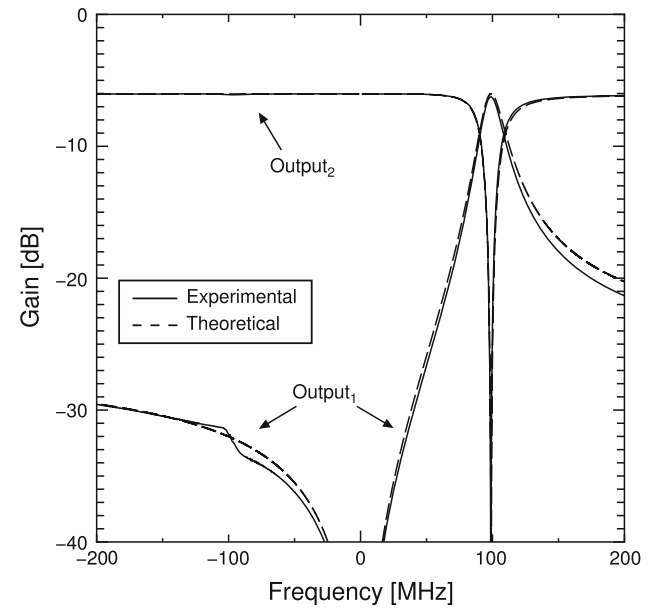

Fig. 10 Experimental results for Type I-A (90–110 kHz)

Figure 10 shows the experimental results. The sign of the frequency is defined by the phase difference between the real and the imaginary input signals. When the phase of the imaginary signal is lagged by 90° with respect to the real signal, it means the positive frequency. Reversely, the negative frequency signal is expressed by leading the phase of the imaginary signal by 90°. In order to apply these signals to the filter under test, a quadrature-phase signal generator will be required.

In this paper, all the frequency responses are examined by using the measurement method based on the principle of superposition [13]. The real and the imaginary signals were separately applied to the filter under test. For an example, the frequency response obtained from Output$_1$ was obtained by the following manner.

1. Measure the frequency response $T_R(j\omega)$ between Output$_1$–Input$_1$. In this measurement, Input$_2$ should be grounded.

2. Measure the frequency response $T_I(j\omega)$ between Output$_1$–Input$_2$. In this measurement, Input$_1$ should be grounded.
3. The frequency response in the positive and the negative frequency areas can be obtained from the following equations:

- $|T(j\omega)| = |H_R(j\omega) + jH_I(j\omega)|$ for positive frequency area
- $|T(-j\omega)| = |H_R(j\omega) - jH_I(j\omega)|$ for negative frequency area

The experimental results agree with the theoretical ones. From Fig. 10, it is found that the proposed circuit has both band-pass and band-elimination characteristics, simultaneously and that they have the same passband edges.

3.2 Proposed circuit using autotransformer (10 MHz)

We designed another complex filter whose operating frequency is 10 MHz. The specifications of the prototype complex filter are

$$\left.\begin{array}{l} \omega_1 = 15 \\ \omega_2 = 5 \end{array}\right\}. \tag{22}$$

In the same fashion as described in Sect. 3.1, we can obtain the resultant filter as shown in Fig. 9. Its element values are $L_1 = L_2 = 0.0666667$, $C_1 = 0.0666667$ and $R_{S1} = R_{S2} = R_{L1} = R_{L2} = 2$.

Next, these element values are scaled such that the operating frequency and the impedance level become 10 MHz and 50 Ω, respectively. The resulting cutoff frequencies are on 6.667 and 20 MHz. The element values of the experimental circuit are summarized in Table 3. The experimental circuit board does not equip the source and the termination resistors because they are already included in measurement instruments. The deviations between the desired and the measured element values are within ±6 %. The transformer is realized by using an iron powder toroidal core T37-6 (Micrometals). This is a bifilar wound transformer and 0.25 mmφ UEW was used. GRM18 (Murata) series chip ceramic capacitors was used. The experimental circuit was implemented on a paper phenolic PCB (t = 1.6 mm).

This circuit is measured in the same way as performed in Sect. 3.1. Unconnected ports are terminated with 50 Ω

Table 3 Element values for experiment 2 (Type I-A, 6.667–20 MHz)

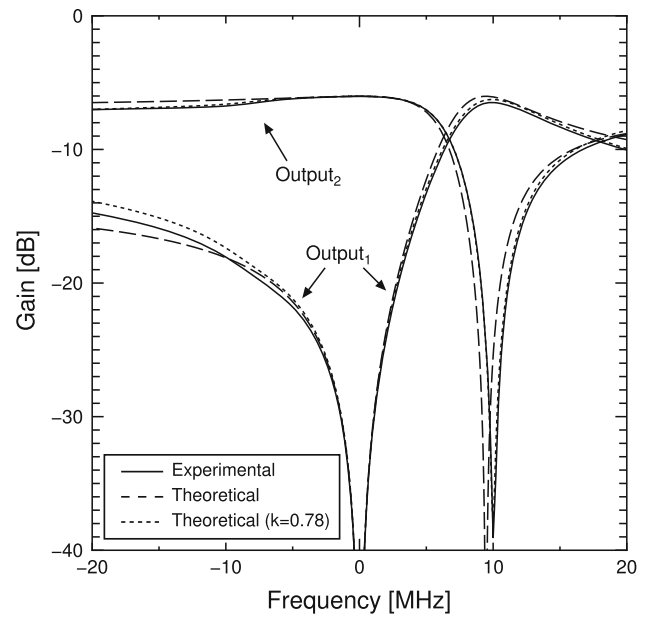| Element	Theoretical	Measured	Turns	Q
C_1	318.3 pF	336.2 pF	–	–
L_1	198.9 nH	210.5 nH	6	73
L_2	198.9 nH	210.1 nH	6	69.5

Fig. 11 Experimental results for Type I-A (6.667–20 MHz)

coaxial terminations. Figure 11 shows the experimental results. In this figure, two theoretical response for $k = 1$ (ideal) and 0.78 are shown. From this figure, the deviation from the theoretical response is due to the coupling coefficient of the autotransformer prepared for experiment.

3.3 Proposed circuit using inductor (100 kHz)

We also designed another complex filter using an inductor. The specifications are

$$\left.\begin{array}{l} \omega_1 \to \infty \\ \omega_2 = \frac{1}{2} \end{array}\right\}. \tag{23}$$

Substituting the above equation set to (3) and (4) yields

$$\left.\begin{array}{l} \omega_0 = 1 \\ \omega_C = 1 \\ x_S = -1 \end{array}\right\}. \tag{24}$$

From Table 1, it is found that the autotransformer shown in Type I-C can be used. Substituting (18) and (24) into (5) gives

$$\left.\begin{array}{l} L' = 1 \\ jR = -j \end{array}\right\}. \tag{25}$$

Figure 12 shows the experimental circuit. Its element values are

$$\left.\begin{array}{l} L = 1 \\ C = 1 \\ R_{S1} = R_{S2} = R_{L1} = R_{L2} = 2 \end{array}\right\}. \tag{26}$$

Next, these element values were scaled such that the operating frequency and the impedance level become
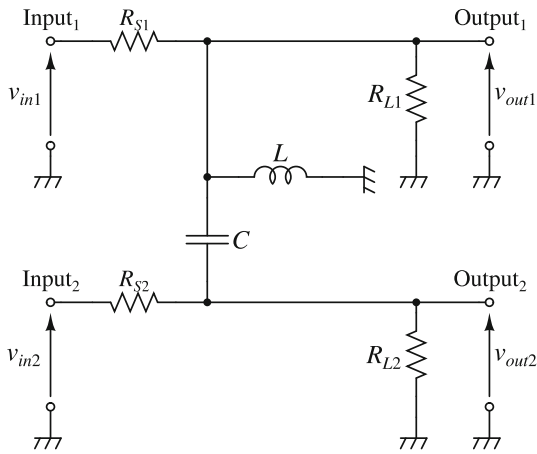
Fig. 12 Experimental circuit using and inductor for Type I-C

100 kHz and 200 Ω, respectively. The resulting cutoff frequencies are on 50 kHz and ∞. Its element values are summarized in Table 4. The deviations between the desired and the measured element values are within ±0.1 %. Figure 13 shows the experimental results. It is difficult to find the difference between the measured and the theoretical responses.

3.4 Proposed circuit using inductor (10 MHz)

The element values given by (25) are scaled such that the operating frequency and the impedance level become 10 MHz and 50 Ω, respectively. The resulting cutoff frequencies are on 5 MHz and ∞. The element values are summarized in Table 5. The deviations between the desired and the measured element values are within ±0.2 %. The circuit is realized in the same way as Sect. 3.3 except the inductor, which is realized by using 1.0 mmϕ solder plated copper wire. Figure 14 shows the experimental results. They agree well with the theoretical ones.

3.5 Monte Carlo simulation

In order to examine sensitivity characteristics of the proposed filters, Monte Carlo simulation was carried out.

Table 4 Element values for experiment 3 (Type I-C, 50 kHz–∞)

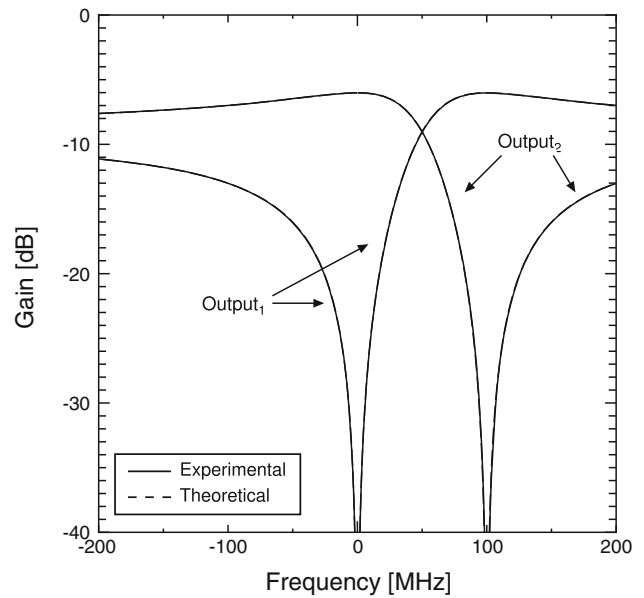| Element	Theoretical	Measured	Turns	Q
R_{S1}	200 Ω	200.0 Ω	–	–
R_{L1}	200 Ω	200.0 Ω	–	–
R_{S2}	200 Ω	200.1 Ω	–	–
R_{L2}	200 Ω	200.0 Ω	–	–
C	15.92 nF	15.92 nF	–	>1,000
L	159.2 μH	159.1 μH	17	212

Fig. 13 Experimental results for Type I-C (50 kHz–∞)

Table 5 Element values for experiment 4 (Type I-C, 5 MHz–∞)

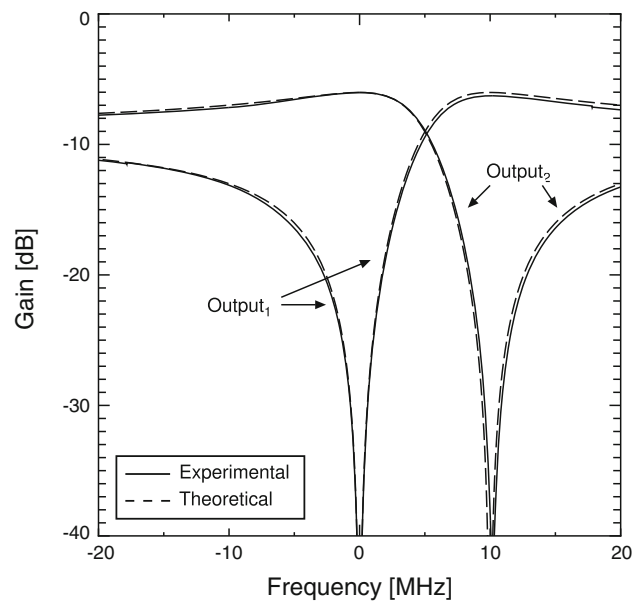| Element	Theoretical	Measured	Turns	Q
C	636.6 pF	636.0 pF	–	–
L	397.9 nH	398.4 nH	6	105

Fig. 14 Experimental results for Type I-C (5 MHz–∞)

Figure 15 shows the simulation results of the circuit for experiment 4. The number of trials is 30. The condition is that the mismatch of the inductor or the transformer and
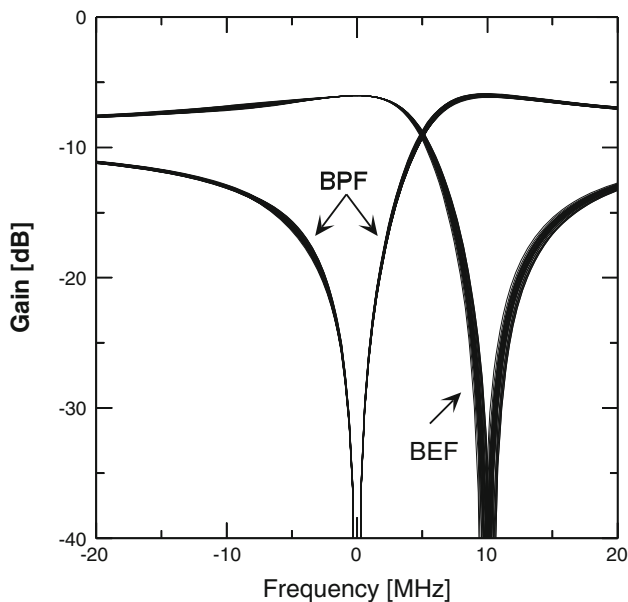
Fig. 15 Monte Carlo simulation of the circuit for experiment 4

the capacitor were set at 5 % in a uniform distribution. The maximum lower passband edge deviation was 4.77–5.21 MHz.

4 Conclusion

In this paper, a passive complex filter which only employs termination resistors, a capacitor and an autotransformer or an inductor has been proposed. The proposed circuit is obtained by equivalently transforming a tight coupling transformer which is included in the conventional circuit. The validity of proposed method is confirmed through experiments.

The further investigation is required to solve the problem that the proposed circuit does not have the imaginary output terminal and that it is difficult to obtain higher-order complex filters.

References

1. Tanaka, A., & Tanimoto, H. (2009). Design of 1 V operating fully differential OTA using NMOS inverters in 0.18 μm CMOS technology. *IEICE Transactions on Fundamentals of Electronics, E92-C*(6), 822–827.
2. Psychalinos, C. (2008). Low-voltage log-domain complex filters. *IEEE Transactions on Circuits and Systems, 55*(11), 3404–3412.
3. Gingell, M. J. (1975). The synthesis and application of polyphase filters with sequence asymmetric properties. Ph.D. Thesis in the Faculty of Engineering, University of London.
4. Crols, J., & Steyaert, M. (1995). A single-chip 900 MHz CMOSreceiver front-end with a high performance low-IF topology. *IEEE Journal of Solid-State Circuits, 30*(12), 1483–1492.
5. Behbahani, F., Kishigami, Y., Leete, J., & Abidi, A. A. (2001). CMOS mixers and polyphase filters for large image rejection. *IEEE Journal of Solid-State Circuits, 36*(6), 873–887.
6. Kaukovuori, J., Stadius, K., Ryynänen, J., & Halonen, K. A. I. (2008). Analysis and design of passive polyphase filters. *IEEE Transactions on Circuits and Systems, 55*(10), 3023–3037.
7. Komoriyama, K., Yashiki, M., Yoshida, E., & Tanimoto, H. (2008). Very wideband active RC polyphase filter with minimum element value spread using fully balanced OTA based on CMOS inverters. *IEICE Transactions on Fundamentals of Electronics, E91-C*(6), 879–886.
8. Shouno, K., & Ishibashi, Y. (2000). Synthesis of a complex coefficient filter by passive elements including ideal transformers and its simulation using operational amplifiers. *IEICE Transactions on Fundamentals of Electronics, E83-A*(6), 949–955.
9. Shouno, K., & Amano, Y. (2012). Passive complex bandpass filter using lossy and loose coupling transformers. *ISCAS 2012*, 2183-2186.
10. Shouno, K., & Ishibashi, Y. (2008). Synthesis of a passive complex filter using transformers. *IEEE Transactions on Circuits and Systems, 55*(7), 1897–1903.
11. Muto, C. (2001). A leapfrog synthesis of passive complex filters based on HPF. *ITC-CSCC2001*, pp. 52–55.
12. Muto, C. (2000). A new extended frequency transformation for complex analog filter design. *IEICE Transactions on Fundamentals of Electronics, E83-A*(6), 934–940.
13. Shouno, K., & Ishibashi, Y. (2002). A note on the measurement method of the frequency response of a complex coefficient filter. In *Electronics and Communications in Japan* (Vol. 85, 6, pt. 3, pp. 32–41). New York: Wiley.

Tomoya Nakagawa was born in Chiba, Japan in 1988. He received B.E. degree in engineering from University of Tsukuba, Japan in 2011. He is currently working toward the M.E. degree in Science and Engineering, University of Tsukuba. His research interests the passive network theory.

Kazuhiro Shouno was born in Tokushima, Japan, in 1971. He received the B.E. and M.E. degrees in engineering from University of Tsukuba, Japan, in 1994 and 1996, respectively. From 1996 to 1998, he worked at Matsushita Electric Industrial Co.,Ltd. From 1998 to 2001, he was engaged in research for a doctor's degree in Engineering, University of Tsukuba. He received the D.E. degree in engineering from University of Tsukuba in 2001. From 2001 to 2003, he was a research assistant in Bio-System Engineering, Faculty of Engineering, Yamagata University. From 2003 to 2010, he was an assistant professor in Institute of the Information Sciences and Electronics, University of Tsukuba. Since 2010, he has been engaged in Graduate School of Systems and Information Engineering, University of Tsukuba, where he is an associate professor. His research interests include passive/active network theory and analog integrated circuit. He is a member of the Institute of Electronics, Information and Communication Engineers (IEICE) of Japan, the Institute of Electrical Engineers (IEE) of Japan and the Institute of Electrical and Electronic Engineers (IEEE) of USA.

Kenji Kuniya was born in Saitama, Japan in 1988. He received B.E. degree in engineering from University of Tsukuba, Japan in 2012. He is currently working toward the M.E. degree in Science and Engineering, University of Tsukuba. His research interests the passive network theory.